45th AIAA/ASME/ASCE/AHS/ASC Structures, Structural Dynamics & Materials Conference
19 - 22 April 2004, Palm Springs, California

AIAA 2004-2056

TEST AND ANALYSIS OF A COMPOSITE MULTI-BAY FUSELAGE PANEL UNDER UNI-AXIAL COMPRESSION

Jian Li
Structural Integrity Department
The Boeing Company
Mesa, Arizona 85215

Donald J. Baker
Vehicle Technology Directorate - ARL
NASA Langley Research Center
Hampton, Virginia 23681

ABSTRACT

A composite panel containing three stringers and two frames cut from a vacuum-assisted resin transfer molded (VaRTM) stitched fuselage article was tested under uni-axial compression loading. The stringers and frames divided the panel into six bays with two columns of three bays each along the compressive loading direction. The two frames were supported at the ends with pins to restrict the out-of-plane translation. The free edges of the panel were constrained by knife-edges. The panel was modeled with shell finite elements and analyzed with ABAQUS® nonlinear solver. The nonlinear predictions were compared with the test results in out-of-plane displacements, back-to-back surface strains on stringer flanges and back-to-back surface strains at the centers of the skin-bays. The analysis predictions were in good agreement with the test data up to post-buckling.

INTRODUCTION

Efforts have been made to demonstrate composite structural technology for rotorcraft primary structures to save weight and cost [1]. However, the cost and weight savings cannot be realized without a better understanding of the structural integrity issues associated with unitized composite structures. A high fidelity failure analysis methodology was previously proposed to analyze unitized composite structures [2]. The objective of this proposed method was to understand the global nonlinear behavior of the entire structure due to the interactions among its components and define local failure modes at the joining locations of the structural components. The high fidelity failure analysis methodology was able to address the limitations of strength based analysis used in the current design methods and identify, before full-scale static tests, potential failure modes missed by traditional strength based analysis [2-3]. The effectiveness of this high fidelity failure analysis methodology needs to be validated by carefully conducted experiments. Therefore, the objective of this paper is to test, under uni-axial compression a panel cut from the Rotary Wing Structures Technology Demonstrator (RWSTD) [1] composite fuselage tool proof article and to model this test article with finite elements. The paper will provide comparison of the model results and the test results in strains and displacements. This paper reports the experimental methods and numerical simulation.

SPECIMEN DESIGN AND EXPERIMENTAL PROCEDURES

A three-stringer multi-bay panel (Fig. 1) was cut from a RWSTD [1] composite fuselage tool proof article (Fig. 2) and made into a compression specimen. The fuselage tool proof article was manufactured from stitched, warp knit, and plain weave, AS4 carbon fiber preforms infused with SI-ZG-5A resin system using vacuum-assisted resin transfer molding (VaRTM) process. The skin was stitched together and the frame and stringer flanges were stitched to the skin. The stringers and frames divided the specimen into six bays with two columns of three bays each along the compressive loading direction. For the remainder of this paper the bays will be identified by their relative location on the test specimen (i.e. upper left, middle right, etc) as shown in Fig. 3 when viewing from the stringer side. The specimen was potted at both ends to facilitate load introduction. The two middle frames were supported at the ends.

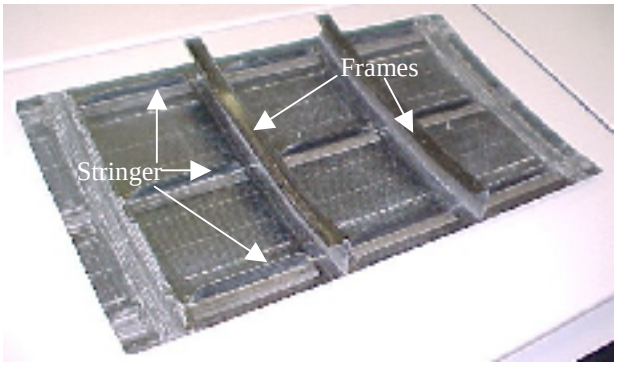

Fig. 1. Three-stringer multi-bay compression specimen.

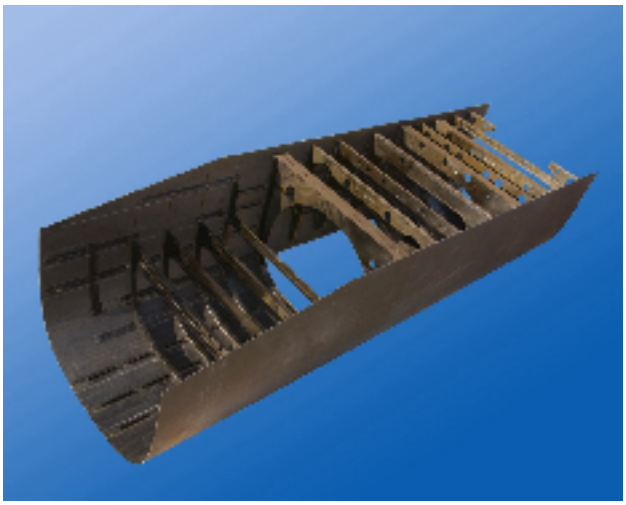

Fig. 2. RWSTD composite tool proof article.

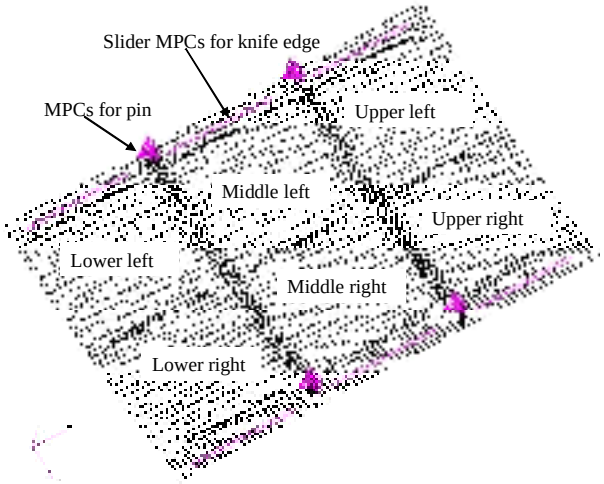

Fig. 3. Analysis model of the compression specimen.

The test panel was instrumented with 42 strain gages as illustrated in Fig. 4. Three pairs of back-to-back axial strain gauges were placed on the stringer flanges at the middle of the three center-stringer segments. Stain gauges 19, 20 and 21 were on the inner mold line (IML) side or the stringer side. Strain gauges 40, 41 and 42 were on the outer mold line (OML) or the surface side. Six pairs of back-to-back rosette strain gages were placed at the centers of the six skin-bays. Each rosette consists of three strain gauges with two strain gages placed to be perpendicular to each other and the third gage is at 45 degrees in between the two perpendicular gages as shown in Fig. 4. The perpendicular gauges were aligned along the vertical and transverse directions and were denoted with strain gauge numbers shown on Fig. 4.

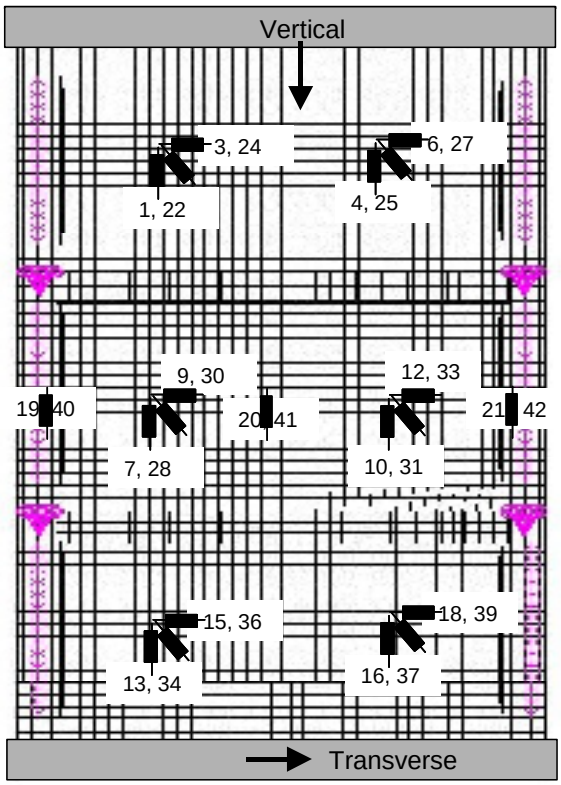

Gauges 1-21 on stringer (near) side
Gauges 22-24 on skin (far) side

Fig. 4. Strain gauges locations and notations.

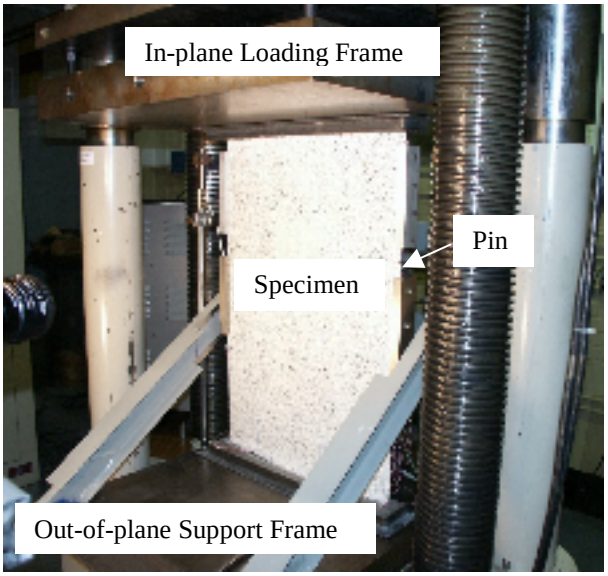

Fig. 5. Compression specimen in loading frame.

The instrumented multi-bay compression specimen with potted ends was placed between the platens of a test machine as shown in Fig. 5. The support for the

frame to react the loads from the frames can be seen in Fig. 5. The specimen surface was painted white for full-field three-dimensional deformation measurement. However, no full-field deformation data will be covered in this paper. A view of the far side, shown in Fig. 6, illustrates the frame used to react the load from restraining the frames ends. The link from the reaction frame to the test panel frames is also shown. After test specimen was installed in the test machine, eight DCDTs were installed on the test machine lower platen to measure deformations at locations illustrated in Fig. 7. Where DCDT's 31 and 32 were used to measure the test specimen end shortening. DCDT's 50 and 57 were used to measure the out-of-plane displacements at the centers of middle left and middle right skin-bays, while DCDT's 51 and 58 were used for displacement measurement at the centers of lower left and lower right skin-bays. Whereas DCTD 15 and 16 measured the out-of-plane displacements on the frame flanges at the specimen centerline, near the stringer terminations as seen in Fig. 7. The specimen was first loaded up to 4.448 KN (1000 lbs) and unloaded to check out the instrumentation. The specimen was then reloaded to beyond initial buckling of the skin-bays but unloaded before any permanent damage was observed. The buckling load was determined by the strain reversal in the back-to-back gages on the skin-bays. The tests were conducted at room temperature.

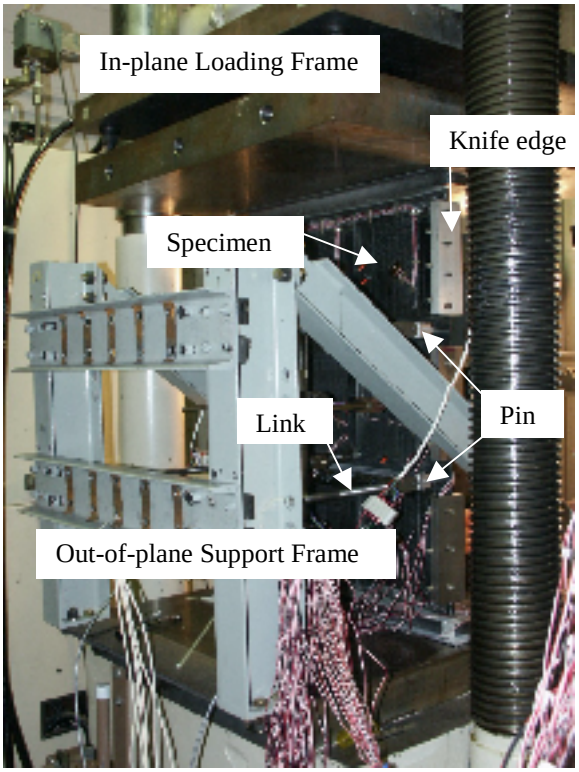

Fig. 6. Pins and knife-edges indicated on specimen.

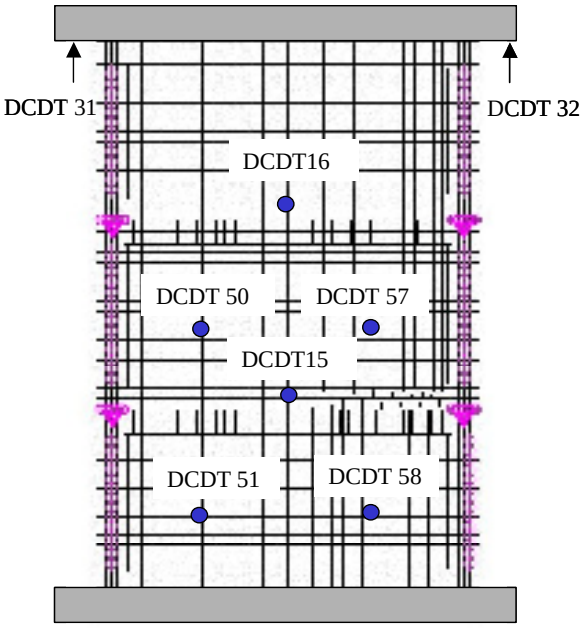

Fig. 7. DCDT notations and locations

MODELING AND ANALYSIS PROCEDURES

The compression specimen was modeled with shell elements as shown in Fig. 3. The pin supports at the frames were modeled with multi-point constraints as shown in Fig. 3. The knife-edge supports were modeled with slider multi-point constraints.

Laminate lay-ups and properties were assigned to each unique regions of the model as shown in Figs. 8 and 9 for skin and stringers/frames, respectively. Where the subscripts "s" and "$" denote mid-plane and mid-ply symmetry for the plies in the parentheses, respectively. The notation $\pm 45^{wk}$ represents two warp knit plies with fibers in ±45 degrees directions, respectively. The ±45 warp knit plies are considered as two plies with each ply thickness as 0.15 mm (0.006 in.). Moreover, 0^{pw} and 45^{pw} represent single plain weave ply with fibers in 0/90 and 45/-45 directions, respectively. In the model, the bi-directional plies are considered as two unidirectional plies with half the plain weave thickness in each direction. Hence, 0^{pw} is considered as 0/90 with nominal ply thickness of 0.1 mm (0.004 in.). Similarly, 45^{pw} is considered as 45/-45 with nominal ply thickness of 0.1 mm (0.004 in.). As an example, the lay-up for the four upper and middle skin-bays $(\pm 45^{wk}/0^{pw})_s$ is input as $(45^{wk}/-45^{wk}/0^{pw}/90^{pw}/90^{pw}/0^{pw}/-45^{wk}/45^{wk})$.

The compression specimen was made from AS4 carbon fiber performs infused with an epoxy resin system, published three-dimensional lamina properties [4] for AS4/3501-6 were used here as an approximation of the actual properties and are shown in Table 1.

Property	Value, Gpa (Msi)
E_{11}	117 (16.7)
$E_{22} = E_{33}$	10.3 (1.5)
$G_{12} = G_{23} = G_{31}$	7.2 (1.04)
ν_{12}	0.27
ν_{23}	0.3
ν_{31}	0.02

The modulus E_{11}=117 Gpa was reduced from Ref. 4 (E_{11}=147 Gpa) to account for the fiber volume fraction difference between the present laminate (52%) and the lamina volume fraction (63%) given in Ref. 4.

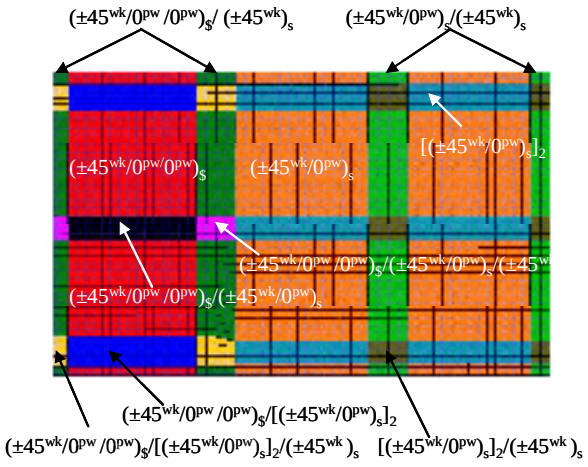

Fig. 8. Color codes and lay-ups for surface regions.

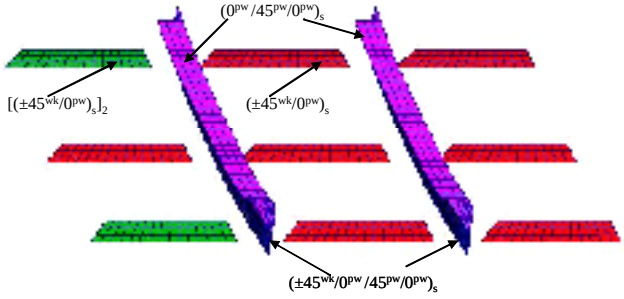

Fig. 9. Color codes and lay-ups for protruding regions.

The panel was analyzed using the finite element analysis program ABAQUS® [5] with geometric nonlinear analysis. The panel was modeled with 3660 thin shell elements, S4R5, with appropriate laminate properties. The selection of thin shell element S4R5 was tested against ABAQUS® moderate thick shell element S4R for the compression specimen. Load-displacement behavior indicated that there was no significant difference between the two shell elements for this application. Mesh density effect was investigated by quadrupling the number of elements in the model. This refinement resulted in less than 10% variation in the peak strain and less than 3% variation in the peak deformation and it was therefore determined that this level of variation was not significant enough to justify the quadrupling of the number of elements for the entire model. The level of mesh refinement shown in Fig. 3 was capable of providing acceptable fidelity in strains and displacements and acceptable turn-around time for analysis.

RESULTS AND COMPARISONS

Load Versus Displacements

Other than the sole correction to E_{11} to account for actual fiber volume fraction, the material properties remain unchanged throughout the analysis process. The DCDT and strain gauge values are unaltered in the comparison charts shown in this section and the following section to ensure an objective and complete blind comparisons.

The overall panel compressive behavior is evident from the load-displacement data measured from DCDT 31 and 32 (Fig. 10). The ABAQUS® geometric nonlinear prediction is also shown in Fig. 10 for comparison with the experimental results. Ignoring the initial knee effects (P/P_{cr} <0.2) shown in the test data, the prediction agrees well with the test data. The figures in this paper will indicate experimental results as solid lines and the nonlinear predictions will be shown as dotted lines. The load axis was normalized by the buckling load (P_{cr}) of the second panel (middle-right) to buckle as shown in Fig. 11. The out-of-plane displacements at the centers of the four skin-bays are shown from Figs. 11 through 14. DCDT 57 (Fig. 11) indicated snap-through buckling of the middle right bay. The skin-bay continuously deformed out to the surface side and then snapped back to the stringer side as the buckling load (P_{cr}) was reached. The nonlinear analysis predicted the buckling well as depicted in Fig. 11. From the results given in Fig. 12, the experimental out-of-plane displacement (DCDT 50) for the middle left bay started to exceed the predicted displacement at 20 percent of the buckling load and continued to exceed prediction by 50 to 60 percent until reaching 90 percent of buckling load. After 90 percent of buckling load, the experimental out-of-plane displacement continued to exceed the nonlinear prediction reaching approximately 300 percent at 140 percent of buckling. The nonlinear analysis was in agreement with the data from DCDT 58 (Fig. 13) and DCDT 51 (Fig. 14) for the two lower skin bays.

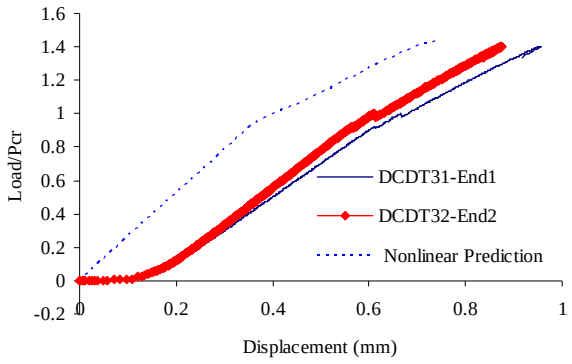

Fig. 10. Comparison of compressive load versus end shortening.

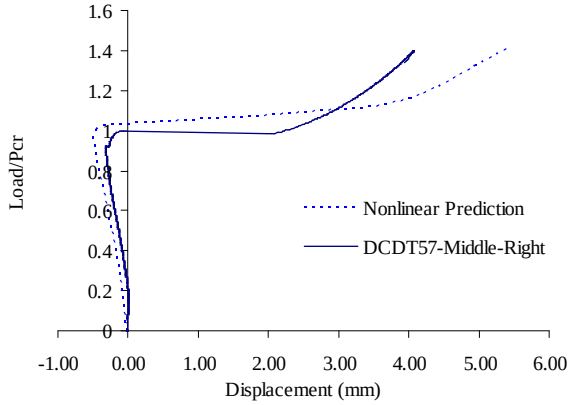

Fig. 11. Comparison of out-of-plane displacement at the center of middle right skin-bay.

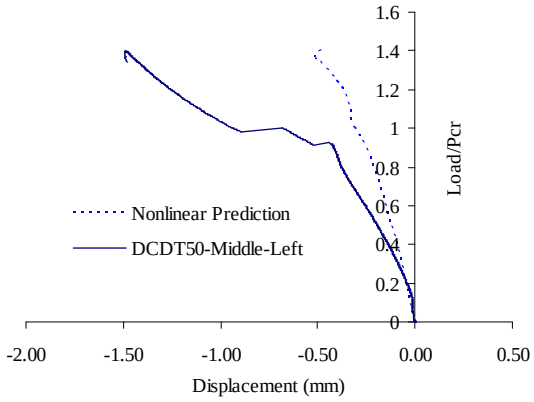

Fig. 12. Comparison of out-of-plane displacement at the center of middle left skin-bay.

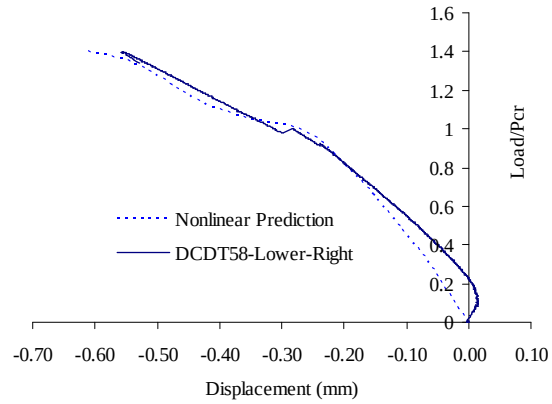

Fig. 13. Comparison of out-of-plane displacement at the center of lower left skin-bay.

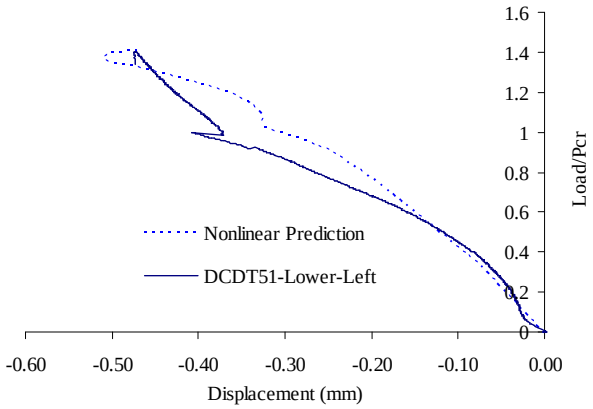

Fig. 14. Comparison of out-of-plane displacement at the center of lower right skin-bay.

Experimental results and nonlinear predictions for the DCDT's located on the frame flanges near the stringer termination are shown in Figs. 15-16. The experimental results indicate the upper frame deflects away from the skin surface starting at 60 percent of the buckling load and reaches the maximum displacement when Load/P_{cr} equals unity before reversing the direction of deflection. The predicted displacement indicates deflection starts at load initiation and continues to a maximum of over 400 percent of the experimental results. Experimentally, the lower frame starts to deflect toward the skin on loading and then reverses deflection direction at approximately 55 percent of the buckling load. The predicted displacement indicates deflection away from the skin on loading and continues on until maximum load. The predicted displacement does match the experimental result from approximately 85 to 100 percent of buckling load.

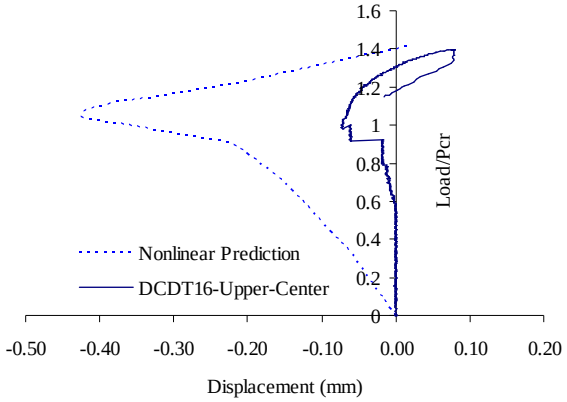

Fig. 15. Comparison of out-of-plane displacement in front of the middle upper stringer termination.

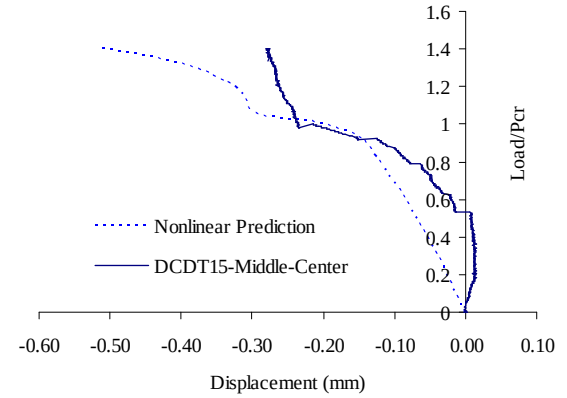

Fig. 16. Comparison of out-of-plane displacement in front of the middle center stringer termination.

Load Versus Strains

Experimental strains in the stringer flanges at the mid-point of the panel are plotted as solid lines in Fig. 17-19. The deviation between the IML and OML strain gages, prior to buckling, indicate a bending in the panel. ABAQUS® nonlinear analysis predictions for the stringer flanges are also shown in Fig. 17-19 as dotted lines with symbols. The nonlinear predictions prior buckling also indicate a bending in the panel. Good agreements occurred between the strain gauge test data and the predictions at those locations. The surface strains in the stringers exhibited near linear response up to near the buckling load (P_{cr}). The nonlinear analysis seems to predict the post-buckling trends as well.

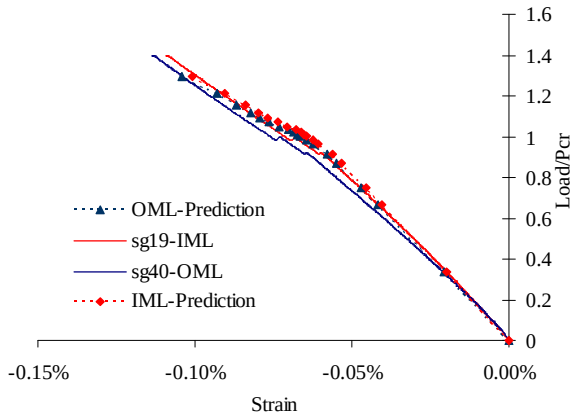

Fig. 17. Comparisons of vertical strains on the middle left stringer flange.

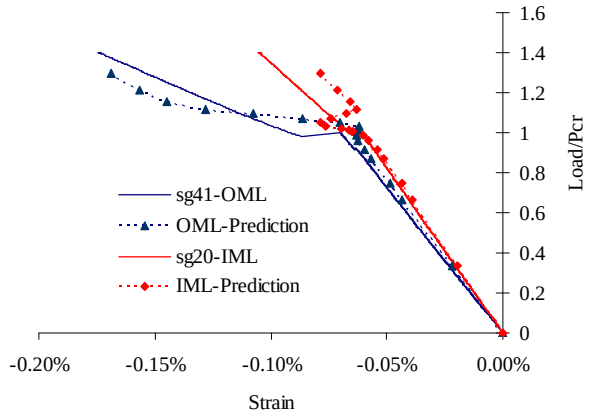

Fig. 18. Comparisons of vertical strains on the middle center stringer flange.

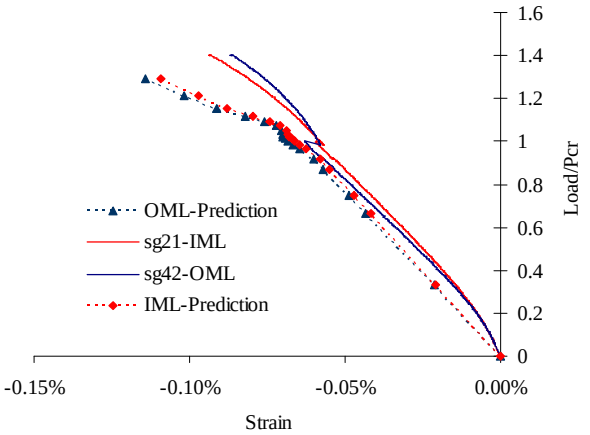

Fig. 19. Comparisons of vertical strains on the middle right stringer flange.

The experimental data from strain gauges in vertical and transverse directions on the IML and OML surfaces

at the six skin-bay centers are plotted as solid lines in Figs. 20-31. The nonlinear predictions at the same locations are plotted as dotted lines with symbols. The experimental axial (load direction) strain and the nonlinear predictions plotted in Figs. 20-21 and 26-27 indicate snap through buckling at the upper left and middle right bays. The strain gauges data shown in Figs. 26-27 confirm the DCDT 57 readings of the out-of-plane displacements shown in Fig. 11. Since there was no DCDT instrumentation for the two upper skin-bays, strain gauges 1 and 24 (Figs. 20-21) on the upper left skin-bay indicated buckling of this bay that otherwise would have been missed. Figures 20-21 also indicates the upper left skin-bay buckled before the middle right skin-bay since the normalized load (by P_{cr} of the middle right skin-bay) at buckling was less than unity. The nonlinear prediction for strain gauges 3 and 24 (Fig. 21) seem to capture the linear region and the buckling load very well. The nonlinear predictions and experimental data from strain gauges 10 and 33 are in very good agreement (Figs. 26-27).

The experimental results and nonlinear predictions at the centers of the four unbuckled skin-bays all indicated the buckling effects of the two buckled skin-bays in the form of drastic changes in the slope of the load versus strain curve. In general, the agreement between the experimental results and nonlinear predictions are good up to these drastic changes as depicted in Figs. 22-25 for the upper right and middle left skin-bays. The predictions and experimental results for the two lower skin-bays seem to agree in trends but differ in magnitudes as shown in Figs. 28-31. However, the agreements in vertical (loading direction) strain components are much better than those in transverse directions as illustrated when Figs. 28 and 30 are compared to Figs. 29 and 31.

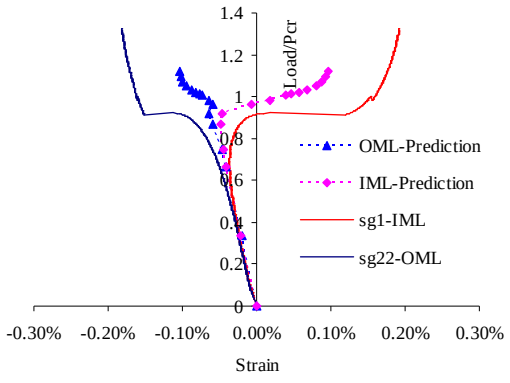

Fig. 20. Comparisons of vertical strains at the center of upper left skin-bay.

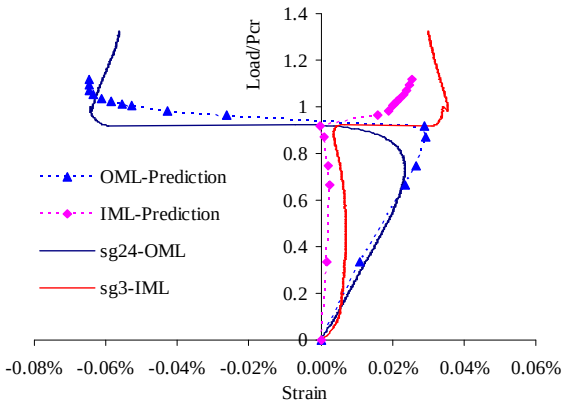

Fig. 21. Comparisons of transversel strains at the center of upper left skin-bay.

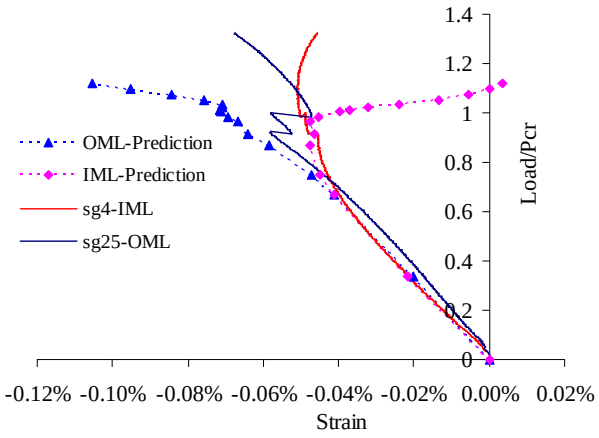

Fig. 22. Comparisons of vertical strains at the center of upper right skin-bay.

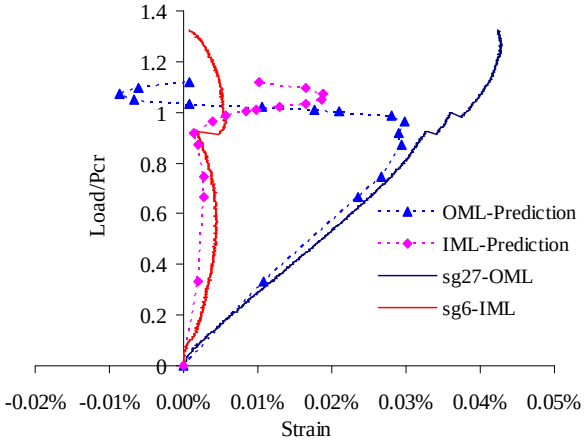

Fig. 23. Comparisons of transverse strains at the center of upper right skin-bay.

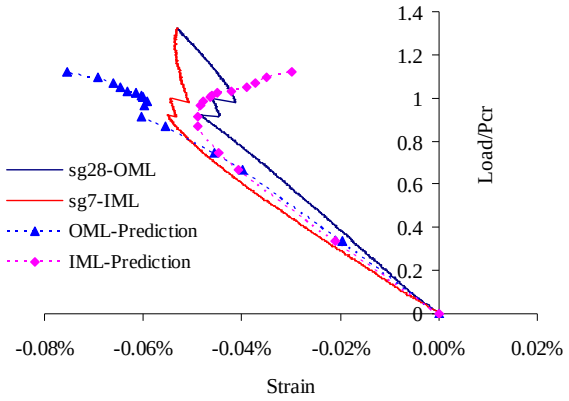

Fig. 24. Comparisons of vertical strains at the center of middle left skin-bay.

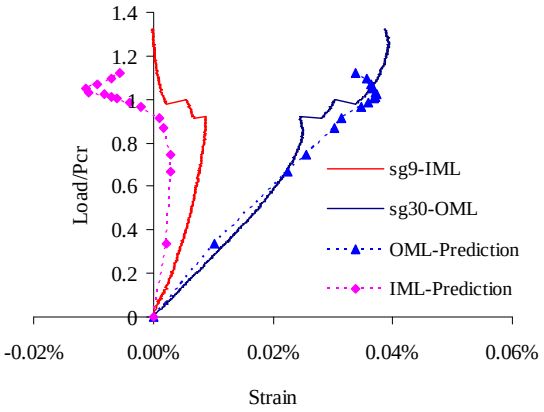

Fig. 25. Comparisons of transverse strains at the center of middle left skin-bay.

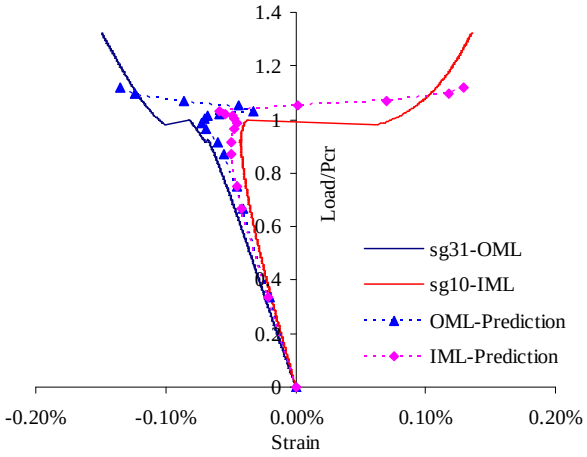

Fig. 26. Comparisons of vertical strains at the center of middle right skin-bay.

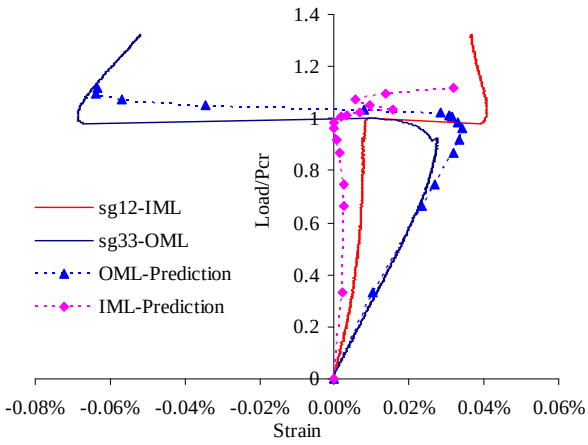

Fig. 27. Comparisons of transverse strains at the center of middle right skin-bay.

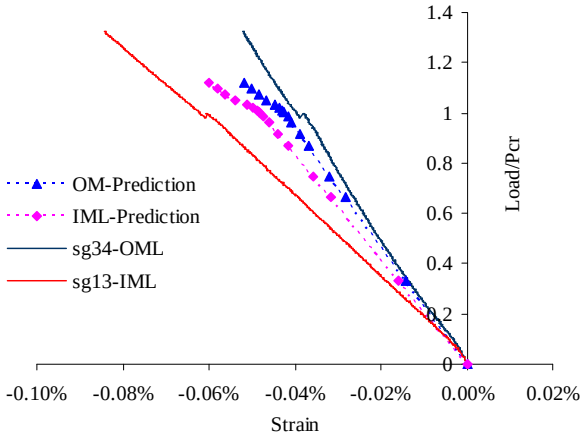

Fig. 28. Comparisons of vertical strains at the center of lower left skin-bay.

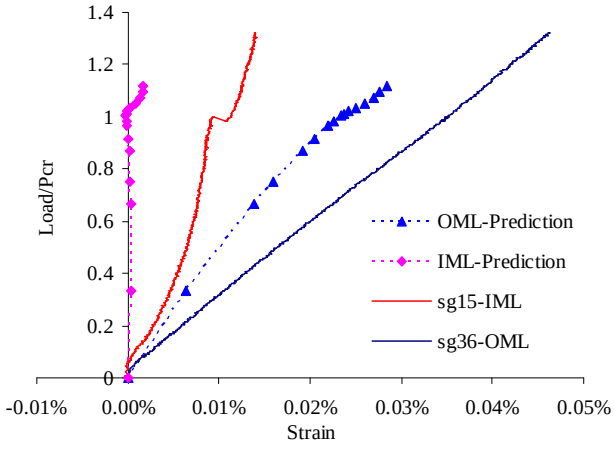

Fig. 29. Comparisons of transverse strains at the center of lower left skin-bay.

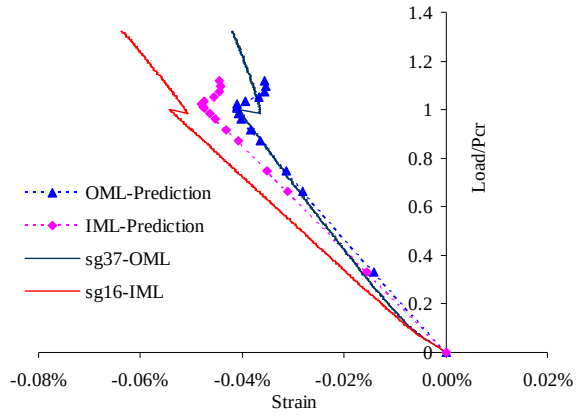

Fig. 30. Comparisons of vertical strains at the center of lower right skin-bay.

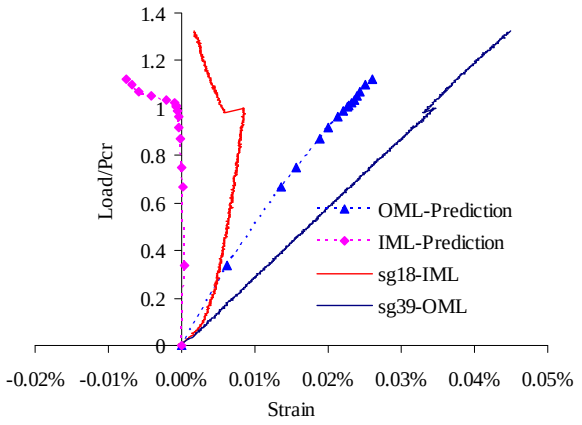

Fig. 31. Comparisons of transverse strains at the center of lower right skin-bay.

DISCUSSION

Testing of a stitched multi-bay carbon-epoxy panel under uni-axial compression and comparing the results to ABAQUS® nonlinear analytical prediction has met the objective of the paper. The experimental data and the nonlinear predictions indicate general agreement in trends from the initial linear region up to and a little beyond the buckling load (P_{cr}) defined previously in this paper. The results shown in Fig. 10-31 indicate a better agreement between experimental results and predictions for the four upper and middle bays than for the two lower bays. The results shown for the four unbuckled bays indicated the load redistribution that occurs when one or more bays buckle. It should be pointed out that complete agreement between test data and predictions for all the strain gauges are not to be expected since imperfections introduced in manufacturing make that impossible. What's remarkable is the fact that the predictions captured the trend in most gauges. Even with less than ideal agreements between some of the experimental results and predictions, the overall performance of the moderate mesh refinement and the ABAQUS® nonlinear solver is excellent in light of the remarkable predictions in displacements and strains and the capture of the essential behavior of the compression specimen. On the other hand, the good agreements between predictions and experimental results also indicate a carefully controlled experimental process.

CONCLUSIONS

The instrumented DCDTs and strain gauges functioned very well as the compression specimen was loaded beyond the snap through buckling regime of two skin-bays. The ABAQUS® nonlinear analysis predicted the locations and the buckling loads and compared very well with experimental results from those two skin-bays. In addition, good agreement between experimental results and ABAQUS® nonlinear analysis predictions were observed in the behavior of the specimen and stringer. The experimental results and associated predictions from the other four, unbuckled, skin-bays were able to capture the buckling effects of the two buckled skin-bays in the form of significant deviations from their existing trends as the buckling occurred. Overall, the level of mesh refinement and the ABAQUS® nonlinear solver captured the panel behavior up to post-buckling. In conclusion the results satisfied the objective of the paper.

ACKNOWLEDGEMENTS

This effort was conducted as part of the Survivable Affordable Repairable Airframe Program conducted under the auspices of the U.S. Army Aviation Advanced Technology Directorate (AATD) at Fort Eustis, VA, and the Rotorcraft Industry Technical Association (RITA) under contract number DAAH10-02-2-0002. We would like to thank George Cowley, Anh Trinh, Ann Cole and David Williams from NASA Langley for their support for the tests.

REFERENCES

1. "Rotary Wing Structures Technology Demonstration," Cooperative Agreement DAAH-10-98-2-002 with U.S. Army Aviation Applied Technology Directorate, Fort Eustis, Virginia, 1998.

2. Li, J., Dávila, C. G. And Chen, T. "High Fidelity Failure Analysis for A Composite Fuselage Section," Proceedings of the American Helicopter

Society 57th Annual Forum, Washington, DC, May 9-11, 2001.

3. Li, J. “High Fidelity Structural Integrity Analysis Methodology for Composite Rotorcraft Structures,” Proceedings of the 48th International SAMPE Symposium and Exhibition, Long Beach, California, May 11-15, 2003, pp. 1430-1440.

4. Daniel, I. M. and Ishai, O., Engineering Mechanics of Composite Materials, Oxford University Press, New York and Oxford, 1994.

5. ABAQUS/Standard User’s Manual Version 6.3.